
Since January 2020 Elsevier has created a COVID-19 resource centre with free information in English and Mandarin on the novel coronavirus COVID-19. The COVID-19 resource centre is hosted on Elsevier Connect, the company's public news and information website.

Sensors & Actuators: B. Chemical 320 (2020) 128351

Contents lists available at ScienceDirect

Sensors and Actuators B: Chemical

journal homepage: www.elsevier.com/locate/snb

# A novel nucleic acid amplification system based on nano-gap embedded active disk resonators

Eun Yeong Lee[a,1], Yeseul Kim[b,1], Bonhan Koo[a], Geun Su Noh[a], Hansuek Lee[b,c,**], Yong Shin[a,*]

[a] Department of Convergence Medicine, Asan Medical Institute of Convergence Science and Technology, Asan Medical Center, University of Ulsan College of Medicine, Seoul, 05505, Republic of Korea

[b] Department of Physics, Korea Advanced Institute of Science and Technology, Daejeon, 34141, Republic of Korea

[c] Graduate School of Nanoscience and Technology, Korea Advanced Institute of Science and Technology, Daejeon, 34141, Republic of Korea

ARTICLE INFO

*Keywords:*
Molecular diagnosis
Optical sensor
Silicon-rich silicon nitride disk
Whispering gallery mode
Point-of-care testing

ABSTRACT

Recent advances in nucleic acid based testing using bio-optical sensor approaches have been introduced but most are based on hybridization between the optical sensor and the bio-molecule and not on an amplification mechanism. Direct nucleic acid amplification on an optical sensor has several technical limitations, such as the sensitivity of the temperature sensor, instrument complexity, and high background signal. We here describe a novel nucleic acid amplification method based on a whispering gallery mode active resonator and discuss its potential molecular diagnostic application. By implanting nanoclusters as active compounds, this active resonator operates without tapered fiber coupling and emits a strong photoluminescence signal with low background in the wavelength of low absorption in an aqueous environment that is typical of biosensors. Our method also offers an extremely low detection threshold down to a single copy within 10 min due to the strong light-matter interaction in a nano-gap structure. We envision that this active resonator provides a high refractive index contrast for tight mode confinement with simple alignment as well as the possibility of reducing the device size so that a point-of-care system with low-cost, high-sensitivity and simplicity.

## 1. Introduction

There are a myriad of nucleic acid detection techniques that utilize mechanical, electrical, electrochemical, or optical sensors for rapid, portable, and cost-effective sensing [1,2]. Diagnostic platforms based on various optical sensors, such as surface plasmon resonance (SPR) [3], surface enhanced Raman scattering (SERS) [4], silicon micro-ring resonator (SMR) [5–7], photonic crystal [8], and whispering gallery mode (WGM) [9–11], have also now been developed for the quantitative and qualitative detection of biomolecules. The features of these sensors include high sensitivity, rapid results, on-site analysis, and multiplexing capabilities. Hence, nucleic acid-based testing techniques that are used as a gold standard diagnostic method in the clinic have been integrated with optical sensors to take advantage of these features. It is notable however that most of the recent advances in nucleic acid testing via optical sensors rely on the hybridization between the biomolecules and the sensors and not on nucleic acid amplification [3,4,9–11]. As nucleic acids typically exist at very low concentrations in clinical samples however [12], the direct combination of an amplification technique and an optical sensor would be hugely beneficial for identifying disease biomarkers that would otherwise be below the threshold of detection.

We have recently developed a one-step isothermal nucleic acid amplification method with bio-optical sensor detection (iNAD) to enable the rapid, simple, and more sensitive detection of biomolecules for various applications [5,6,12,13]. Our iNAD methodology combined an SMR biosensor and recombinase polymerase amplification (RPA) enzyme to simultaneously amplify and detect nucleic acids via refractive index changes in a label-free and real-time manner [5,6,12,13]. Despite the obvious advantages of iNAD however, it had some notable limitations in relation to molecular diagnostics such as the complex alignment between optical fiber and resonator, use of an expensive tunable laser, the small shift range of the resonant wavelength, and a high background signal [6]. These limitations of iNAD are inherited from the

* Corresponding author.
** Corresponding author at: Department of Convergence Medicine, Asan Medical Institute of Convergence Science and Technology, Asan Medical Center, University of Ulsan College of Medicine, Seoul, 05505, Republic of Korea.
*E-mail addresses:* hansuek@kaist.ac.kr (H. Lee), shinyongno1@gmail.com, shinyongno1@amc.seoul.kr (Y. Shin).
[1] These authors contributed equally.

https://doi.org/10.1016/j.snb.2020.128351
Received 10 February 2020; Received in revised form 15 May 2020; Accepted 21 May 2020
Available online 26 May 2020

conventional resonance-shift sensing scheme based on high-Q resonators rather than iNAD technique itself. Although the narrow resonance linewidth of high-Q resonators provides high resolution to measure small wavelength shifts induced by detection events, it requires narrow linewidth tunable lasers and complicated coupling scheme to access the resonance mode [9]. In addition, it is sensitive not only to detection events but also to any environmental perturbations such as thermal fluctuation [14]. To overcome these restrictions, we recently developed active WGM sensors that employed two nanostructures, namely silicon nanoclusters and nano-gap [15]. In this sensor, by means of efficient luminescent of silicon nanoclusters, resonance mode can be remotely excited by fixed-wavelength lasers or LEDs and also remotely read out through free space without physical connections to the external measurement setup. Furthermore, optical field confined in extremely small area of nanogap magnifies resonance shift selectively to the target events which occurred in the gap. Although the operation of this WGM sensor with practical impacts has been validated for detection of streptavidin-biotin complexes [15], the possibility of nucleic acid amplification directly on the surface of these resonators has not been explored as the sensitivity and specificity of the technique has needed further improvements.

We here describe for the first time a novel nucleic acid amplification system based on nano-gap active resonators that can be used for in various molecular diagnostic applications, which requires a label-free and real-time detection with rapidity and high sensitivity. This platform is combined with RPA as the isothermal nucleic acid amplification enzyme in order to specifically detect the target nucleic acids without the need for a complex thermal instrument. Crucially, this novel system overcomes the limitations of combining a nucleic acid amplification mechanism with an optical sensor. These include the temperature sensitivity of the sensor, instrument complexity, complex alignment, and high background signals. The active resonator used in our new system does not require direct physical contact for coupling of the waveguide and optical fiber. In addition, no background signal is obtained from non-specific binding using the active resonator. A low concentration target sample is therefore easily distinguishable from the non-target molecules, thus enhancing the detection sensitivity. We have now used our novel method to detect Middle East respiratory syndrome-coronavirus (MERS-CoV), Zika virus (ZIKV), and *Brucella ovis* with high sensitivity and specificity within 10 min and with a 100-fold higher sensitivity than conventional PCR methods. We discuss the wider applicability of this method for detecting known pathogens and disease biomarkers.

## 2. Experimental section

### 2.1. Fabrication of silicon-rich silicon nitride disk as a biosensor

The detailed design and fabrication processes for the nano-gap disk resonator have been described previously [15]. Briefly, the performance enhancement of the developed sensor is achieved by introducing two nanostructures to WGM resonators: silicon nanoclusters and a nano-gap. The WGM resonances are excited by nanoclusters emitting a strong photoluminescence (PL) in the 700 nm wavelength range where the absorption by water remains low. To form silicon nanoclusters uniformly in a resonator, silicon-rich silicon nitride (SRSN) film is deposited on a substrate and fabricated into disk resonators. The excess silicon changes into silicon nanoclusters via a post-annealing process performed in an argon environment. A nano-gap structure is introduced in the resonator by placing two pieces of the silicon nitride disk plates in 25 nm distance. During the sensing experiment, the gap is filled with mixture in DI water having a lower refractive index (n = 1.33) than that of silicon nitride (n = 2) disk plates. For the continuity of the electric field at the boundary, the large refractive index contrast in 25 nm gap strongly confines the field intensity in it, which strongly enhances light-matter interaction. For the operation of the SRSN disk resonator as a biosensor, the wafer chips having the SRSN disk resonators were prepared in three steps. First, the surface of the chip was functionalized with an amine group for immobilization of the primer, as an asymmetric technique. The chips were then treated with $O_2$ plasma and immersed in a solution of 2% 3-aminopropyltriethoxysiane (APTES, Sigma-Aldrich) in a mixture of ethanol–$H_2O$ (95:5, v/v) for 2 h, followed by thorough rinsing with ethanol and deionized (DI) water. The SRSN disks chips were cured by drying under nitrogen gas and heating to 120 °C for 15 min. Second, the SRSN disks were incubated with 2.5 % glutaraldehyde (GA, Sigma-Aldrich) in DI water containing 10 mM sodium cyanoborohydride for 1 h, rinsed with DI water, and dried under nitrogen gas. Third, forward primers were immobilized to target specific primers containing the 5′ amino-modifier C12. The pretreated disk was prepared by overnight incubation at room temperature with 1 μM of forward primers in 50 mM 2-(*N*-morpholino) ethanesufonic acid solution (MES, adjusted pH 6.0) containing 20 mM sodium cyanoborohydride. After this incubation, unbound target specific primers were removed by washing with 50 mM MES solution (pH 6.0) and the disks were dried using nitrogen gas. The primer-immobilized SRSN disks chips were stored at room temperature until further use. To test the target amplification and detection by the primer immobilized SRSN disk, recombinase polymerase amplification (RPA, TwistDx, Cambridge, UK) or recombinase polymerase amplification-reverse transcription (RPA-RT, TwistDx, Cambridge, UK) was conducted in a mixture of 59 μL of rehydration buffer, 30 μL of RNase-free DI water, and 10 μL of reverse primer (10 μM). Two dried enzyme pellets were added to each solution and vortexed, and 5 μL of magnesium acetate solution was added. To start the reaction, 40 μL of RPA or RPA-RT solution and 10 μL of target DNA or 20 μL of target RNA were mixed. Next, 50 μL or 60 μL of this mixture was injected into the inlet of the microfluidic channel by a syringe pump and guided to the disk array located in the middle of the channel. The SRSN disk resonator sensor assay was operated at a constant temperature (38 °C for DNA and 43 °C for RNA). The photoluminescence spectra were measured every 5 min for up to 30 min to monitor the immobilized amplification of target nucleic acids in a label-free and real-time manner.

### 2.2. Pathogen cultures for DNA preparation

*Brucella ovis* (ATCC 25840) was grown in trypticase soy broth (TSB, BD Difco) containing 5% defibrinated sheep blood (MBcell, Korea) and incubated at 37 °C in an atmosphere of 5% $CO_2$ for 48 h. *Salmonella enterica* (ATCC 14028) was inoculated into nutrient broth (NB, BD Difco) and incubated for 24 h at 37 °C under an aerobic atmosphere. After culturing, bacterial suspensions were quantified using the agar plate method and subsequently diluted to different concentrations in PBS [16]. DNA was then extracted from the cultivated samples using a QIAamp DNA Mini Kit (Qiagen, Hilden, Germany).

### 2.3. T7 in vitro transcribed RNA preparation

T7 *in vitro* transcribed RNA of ZIKV and MERS-CoV was generated to assess the detection ability of the SRSN disk resonator assay using the MEGAscript T7 kit (Ambion, Thermo Fisher Scientific, Waltham, MA). For ZIKV, we used the QIAamp viral RNA mini kit (Qiagen, Hilden, Germany) to extract RNA from the medium of the NATtrol Zika Virus. NATZV is an External Run Control-containing strain of MR766 (Zeptometrix Corporation, Franklin, MA), which was formulated with purified, intact virus particles that had been chemically modified to render them non-infectious and refrigerator-stable. The amplicons of ZIKV generated in the end-point reverse transcriptase (RT)-PCR assay were used to create the T7 in vitro transcribed RNA [6]. Synthetic RNA transcripts were purified with a MEGAclear Kit (Ambion, Thermo Fisher Scientific) and quantified using a Nanodrop spectrophotometer (Thermo Fisher Scientific). The purified T7 RNA of ZIKV was stored at −80 °C until use.

### 2.4. Conventional PCR

We performed end-point PCR to determine the quality of the isolated DNA and end-point RT-PCR to determine the quality of the extracted RNA [6,16]. The PCR cycling conditions consisted of an initial denaturation step at 95 °C for 15 min; 40 cycles at 95 °C for 30 s, 58 °C for 30 s and 72 °C for 30 s; and a final extension step at 72 °C for 7 min. In each reaction, a 5 μL aliquot of DNA was amplified in a total volume of 25 μL containing PCR buffer (10X, Qiagen), 2.5 mM $MgCl_2$, 0.25 mM deoxynucleotide triphosphate, 25 pM of each primer, one unit of Taq DNA polymerase (Qiagen) and deionized (DI) water. For the RNA assays, 5 μL of isolated RNA was amplified in a total volume of 25 μL containing One-step RT-PCR buffer (5X, Qiagen), 0.25 mM deoxynucleotide triphosphate, 25 pM of each primer, 1 μL of RT-PCR One-step enzyme mix (Qiagen) and DI water. The following thermal profile was used for RT-PCR: 30 min reverse transcription at 50 °C; 15 min predenaturation at 95 °C; 40 cycles of 30 s at 95 °C, 30 s at 60 °C, and 30 s at 72 °C; and a final extension at 72 °C for 10 min. The resulting PCR and RT-PCR products were separated on 2% agarose gels containing ethidium bromide (EtBr) and imaged with a Gel-Doc System (Clinx Science Instruments, Shanghai, China).

## 3. Results and discussion

### 3.1. A nano-gap embedded active resonator for nucleic acid amplification

The principle of our novel active resonator-based nucleic acid amplification sensor for ultrasensitive molecular diagnostics is illustrated in Fig. 1. To overcome the limitations of existing methods such as the lack of rapidity, low-sensitivity, and requirement for a bulky instrument for optical and thermal cycling, we adopted several recently described techniques. First, SRSN active disk resonators were used as photoluminescence sensors for the PL peaks generated by the direct amplification of nucleic acids on the sensor surface in a label-free and real-time manner. Second, recombinase polymerase amplification (RPA) was used to amplify target nucleic acids under isothermal conditions in the nanogap structure of the active disk resonators where light-matter interaction was greatly enhanced (Figs. 1 and 2a). Third, specific target primers were grafted onto the resonator surface as an asymmetric amplification method for direct amplification of the DNA with no hybridization reactions used. A microfluidic channel was then used to streamline the amplification processing. The microfluidic channel comprises slide glass as a transparent window through which the pump and emission light passes and acrylic foam for the main body structure through which needles are inserted to connect the inflow and outflow tubes (Fig. 2b). After the assembly of the microfluidic channel on the resonator and operating system (Fig. 2b), a mixture of the target nucleic acids (either DNA or RNA) and RPA solution is injected into the microfluidic channel. The recombinase enzyme from the RPA recognizes the primers and facilitates the formation of recombinase-primer complexes. These complexes bind to the target nucleic acids and enable the strand exchange which will begin the amplification process both on the surface of disk resonator (solid) and solution simultaneously (Fig. 1-rectangle), with the temperature maintained at isothermal conditions (38 °C or 43 °C for DNA or RNA, respectively).

The target nucleic acids are thereby amplified on the disk surface and the resulting amplicons are detected by measuring the PL peak shifts generated by the interaction of the target nucleic acid amplification on the surface of the disk resonator and the resonance mode. Due to the large absorption cross-section of silicon nanoclusters in the SRSN, a pump beam of 0.5 mW at a 457.9 nm wavelength from the Ar-ion laser is sufficient to induce photoluminescence spectrum peaks along with the resonance modes of the SRSN resonator. The focusing area of the pump beam is 12,500 $\mu m^2$, and the focusing beam density on the focal plane is 4 $W/cm^2$. The photoluminescence emissions from the excited resonator are collected by an objective lens and selectively captured by a polarizer for TM (transverse magnetic) modes which are strongly confined to the nano-gap (25 nm). Lastly, the signal is detected by a CCD (Charge-coupled detector) and spectrometer (Acton sp2500) through free-space optics without the need for direct physical contacts for coupling such as tapered fibers. Here, we designed the experiment to pump only one resonator and measured the signal generated from this excited single resonator. This remote pumping and detection scheme overcomes the problems with adjusting the optical fiber to the waveguide for a silicon micro-ring resonator.

In order to characterize the temperature rise effect separated from the sensing signal, the center wavelength of the TM fundamental mode was measured while increasing the power of the pump beam. As shown in Fig. S1, the resonance mode began to be observed through the spectra from 0.64 $W/cm^2$ of the pump intensity, and there was no peak shift even when the beam power was increased to the maximum power of the Ar-ion laser, which is 4 times larger than the pump power used in the sensing experiment. Hence, there is no significant temperature increase that is enough to affect the resonant peak shift during the sensing experiment. The target nucleic acids can thus be detected within a few minutes using these photoluminescence resonators in a label-free and real-time manner.

### 3.2. Fundamental characterization of the photoluminescence resonator

We first determined the optimal protocol for using the photoluminescence resonator for nucleic acid sensing. These resonators were fabricated under specific conditions including a 12 μm diameter of the microcavity and a 25 nm thickness of the nano-gap stretched over 1 μm depth from the disk edge to the radial direction. The inset in Fig. 2a is a magnified image of the yellow dotted region clearly showing a 25 nm gap between the two separate disks. By simultaneously considering sensitivity enhancement, fabrication issues, and the sizes of the molecules, we designed a 25 nm gap, which provided a sensitivity of about 6.5 times higher than the structure without the nano-gap (Fig. S2). The measurement set up used in this study is depicted in Fig. 2b. The measured spectra in the aqueous environment show fundamental TM modes, and the quality factor attained from the fitted Lorentzian function is 5500 at 719.55 nm (Fig. 3a). By numerical calculations using COMSOL multi-physics, we confirmed that 8.6 % of the total energy of TM fundamental mode is confined in the nano-gap structure. Consequently, the target DNAs amplified in this gap strongly interact with the confined mode, which increases the sensitivity of the sensor by 6.5-fold compared to a micro-resonator with no nano-gap [15]. Fig. S3 shows the relative E-field intensity profile of the nano-gap disk resonator. Next, for the direct amplification of nucleic acids on the surface of the resonator, we examined whether the peak shift depends on the temperature. Although the peak could be shifted by increasing the temperature from ambient to 38 °C, the peak was found to be stable once a specific temperature was reached (Fig. 3b). Using this optimized protocol, the target nucleic acids were successfully amplified on the resonator surface. In addition, the PL peak is be measured every 5 min for up to 30 min during amplification processing (Fig. 3c). After the surface treatment, the Q- factor of the resonance mode decreased on average from 5500 to 1300. That is, the Q factor was reduced by about 4 times as it went through the process of disk surface treatment with the primer. After the primer was attached and reacted with the actual target DNA, the change in the Q-factor was traced over time (Table S1). Hence, the surface treatment of the original resonator reduced the value of the Q-factor, but the subsequent binding to the surface and amplification process did not significantly affect the Q-factor reduction.

To confirm that the DNA was diffused into the nano-gap and detected in a strong E-field within the gap, we analyzed the sensitivity of the TM and TE (transverse electric) fundamental modes. The surface sensitivity of the nano-gap disk resonator calculated with the finite element method (FEM) simulation of the TM mode was measured at 1.42 nm/nm, which is 3.4 times higher than that of the TE mode of

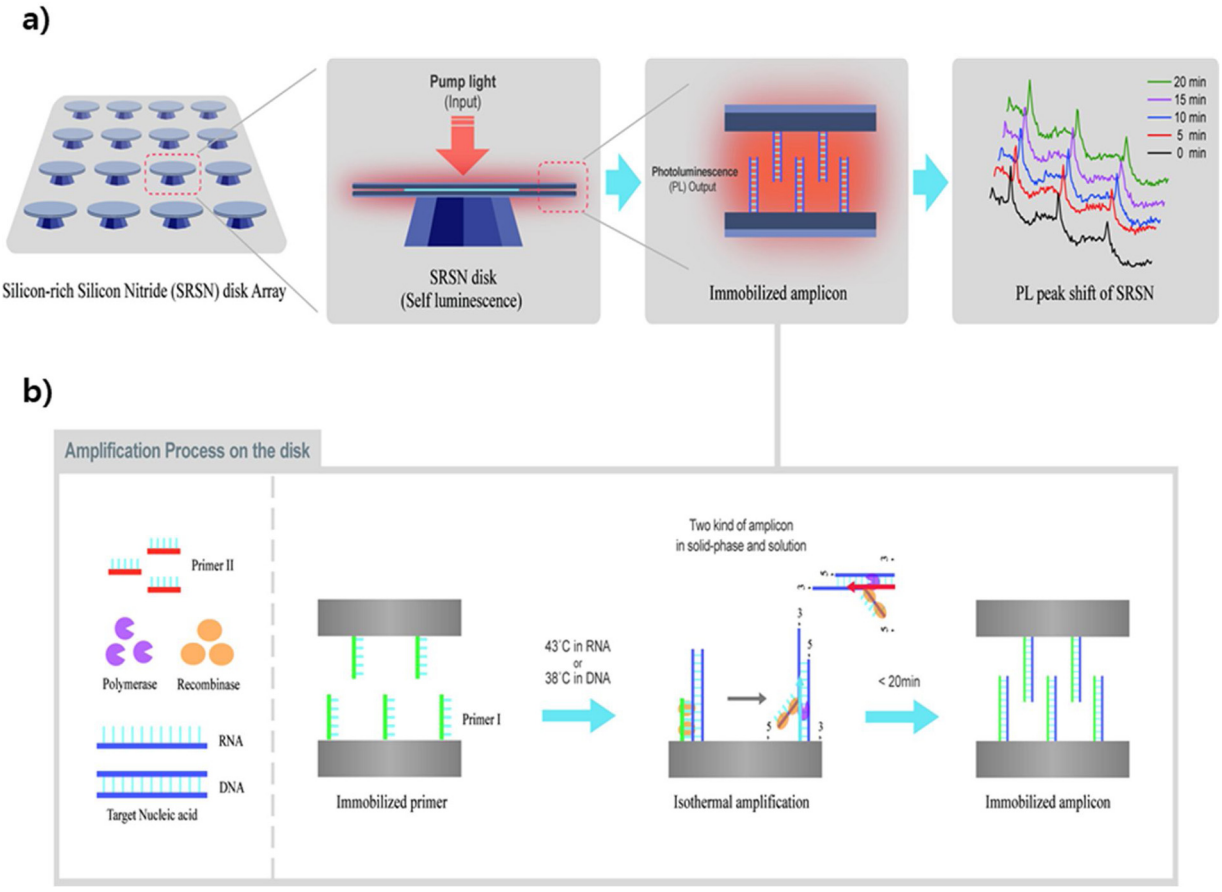


**Fig. 1.** Schematic representation of the silicon-rich silicon nitride (SRSN) based nano-gap embedded active resonator as a molecular diagnostics system. a) The optically pumped resonator emits side photoluminescence (PL) in the 700 nm wavelength range where absorption by water is low. The embedded nano-gap between the two parallel disk plates confines the E-field, which can enhance sensitivity by increasing the light-matter interaction. The target nucleic acid (NA) amplification in this gap is detected immediately by monitoring the wavelength shift of resonant peaks in the PL spectrum. b) Recombinase polymerase amplification (RPA) based on disk amplification. One primer is immobilized on the surface of the resonator and the RPA solution includes the other primer and target nucleic acids. Using an isothermal environment (38 ˚C or 43 ˚C for the DNA or RNA sample, respectively), primer-recombinase (orange) complexes bind to their target nucleic acids and facilitate strand exchange. The immobilized primers are extended by polymerase (purple) on the surface of the resonator. Two kinds of amplicon, in solid-phase and in solution, are formed and exponential NA amplification on the solid phase is achieved by the repetition of the process. During the amplification reaction, detection of the target NA was monitored simultaneously by measuring the resonance peak of the resonator. (For interpretation of the references to colour in this figure legend, the reader is referred to the web version of this article).

0.41 nm/nm. In this calculation, it was assumed that *Brucella* DNA was uniformly attached to the entire resonator surfaces, i.e. inside and outside of the gap. In contrast, by restricting the reaction only to the outside of the gap, the calculated sensitivity of TM mode stayed at twice that of the TE mode. In the *Brucella* DNA detection experiment, the peak shift in the TM mode was 0.349 nm, which is 3.4 times higher than the TE mode. As a result, it can be confirmed that target DNA was uniformly attached to the entire surface of the resonator, including the surface in the nano-gap (Fig. S3).

### 3.3. Bacterial DNA amplification using the photoluminescence resonator

We determined the limit of detection of the photoluminescence resonator for bacterial DNA amplification using *Salmonella enterica and Brucella ovis* as the test pathogens. The size and concentration of the primers on the resonator had been determined in our previous studies

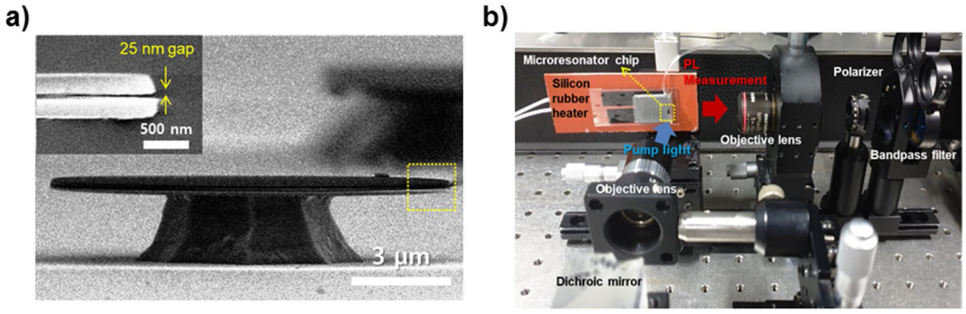


**Fig. 2.** Nano-gap disk resonator and Setup. a) Scanning electron microscope (SEM) image of a disk resonator having 12 μm diameter. Inset: magnified image of the yellow dotted region clearly showing a 25 nm gap between two separate disks. b) Photograph of the experimental setup. The nano-gap disk resonator is in a microfluidic channel into which an argon (Ar)-ion laser beam is pumped from the top. PL emissions are collected by an objective lens, from which the transverse magnetic (TM) mode is selectively captured by a polarizer. (For interpretation of the references to colour in this figure legend, the reader is referred to the web version of this article).

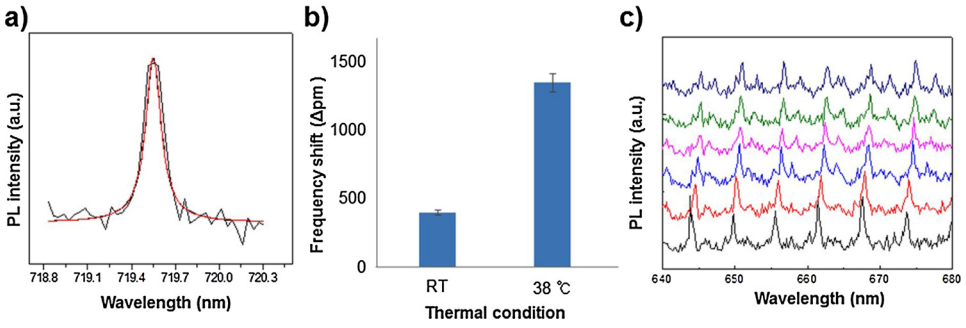


**Fig. 3.** Features of the nano-gap disk resonator. a) Experimental spectra and their Lorentzian fittings for a selected WGM. The resonance wavelength and quality factor of the mode attained from the fitted Lotentzian function are 719.55 nm and $5.5 \times 10^3$, respectively. b) Wavelength shifts and fluctuations at room temperature and temperature controlled conditions with the same concentration of *Brucella Ovis* DNA ($10^6$ copies/reaction). c) PL spectrum of the nano-gap disk resonator. A wavelength shift in the resonant mode is induced by amplification of bacterial DNA from *Brucella Ovis* ($10^5$ copies/reaction). The colors indicate the turnaround time of the isothermal amplification reaction i.e. black (0 min), red (5 min), blue (10 min), pink (15 min), green (20 min) and dark blue (30 min). (For interpretation of the references to colour in this figure legend, the reader is referred to the web version of this article).

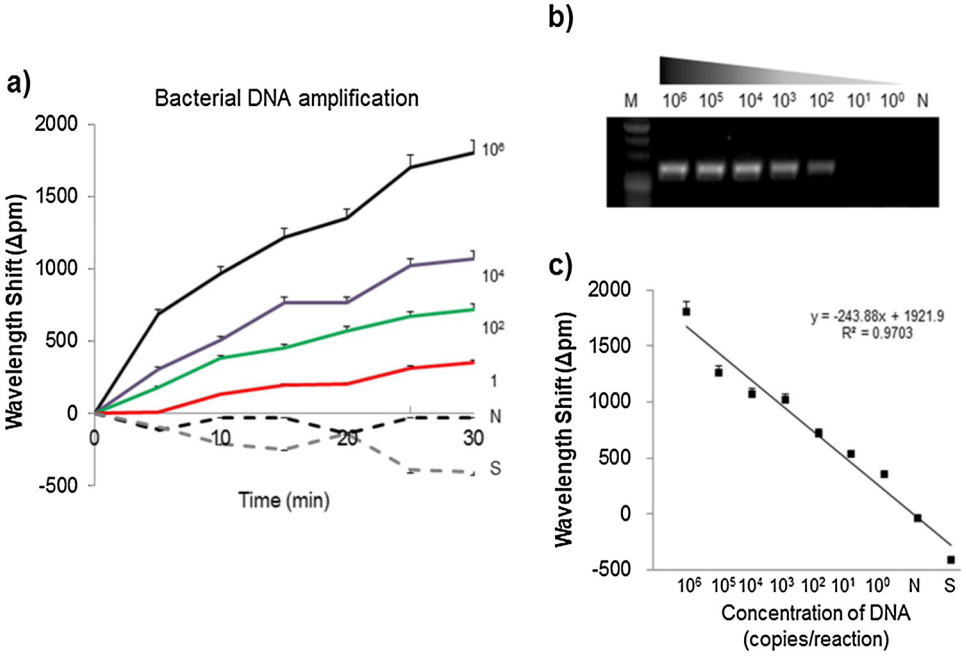


**Fig. 4.** Limit of detection of the nano-gap disk resonator for bacterial DNA amplification. a) A wavelength shift of the resonant mode is induced by serial dilutions of *Brucella Ovis* DNA: black ($10^6$ copies/reaction), purple ($10^4$ copies/reaction), green ($10^2$copies/reaction), red (1 copy/reaction), black-dot (negative control with no DNA), and gray-dot (negative control containing *Salmonella enterica* DNA). b) Gel electrophoresis of 212 bp products generated by conventional PCR. M, 100bp marker; N, negative control with no DNA). c) Linear relationship between the wavelength shift in the resonant mode and the target DNA concentration within 30 min of the reaction commencement. Error bars indicate the standard error of the mean based on at least three independent experiments. (For interpretation of the references to colour in this figure legend, the reader is referred to the web version of this article).

[6,16]. DNA from *B. ovis* was obtained from a spin-column kit and prepared at varying concentrations from 1 to $10^6$ copies/reaction (Fig. 4). The RPA-based reaction mixture used for the isothermal amplification on the resonator was prepared in a tube at room temperature by pipetting. Aliquots of 50 μL of the reaction mixture, including 10 μL of sample DNA, were then injected in the microfluidic channel integrated with the SRSN disk resonator. While the temperature was kept constant at 38 °C, the resonance peaks were shifted by amplification of the target DNA on the disk resonator surface. Using the resonator, the target DNA from *B. ovis* could be clearly identified within 30 min compared to non-targets from either *S. enterica* or distilled water (Fig. 4a). Moreover, we successfully distinguished qualitatively between positive (*B. ovis*) and negative (*S. enterica* and DI water) samples within 10 min using the resonator due to the extremely low background signal in the negative controls.

We compared the limit of detection between our new resonator and a conventional PCR method using serially diluted *B. ovis* bacterial DNA samples ranging from 1 to $10^6$ copies/reaction (Fig. 4). The resonance peak shifts increased proportionally from 1 (353.33 pm, red) to $10^6$ (1801.33 pm, black) copies/reaction and were clearly distinguishable from deionized water (no template control, black dot) and an *S. enterica* DNA sample (non-target control, gray dot) (Fig. 4a). Using conventional end-point PCR however, we could not observe the 212 bp amplicon indicating *B. ovis* positivity at a dilution below $10^2$ copies/reaction (Fig. 4b). As indicated in Fig. 3c, a good linear relationship ($R^2 = 0.9494$) was found between the wavelength shift and different concentrations of the target at 30 min. Notably also, the limit of detection of the SRSN disk resonator for bacterial DNA amplification was 100-fold more sensitive than that of the conventional PCR method (Fig. 4).

### 3.4. Viral RNA amplification using the photoluminescence resonator

We next examined whether the SRSN disk resonator system could also sensitively amplify RNA from virus samples (Fig. 5). To optimize the resonator for this purpose, T7 RNA transcripts from a MERS-CoV and Zika virus (ZIKV) sample were prepared. Forward primers specific for these RNAs were immobilized onto the surface of the disk slot, followed by the addition of reverse transcriptase (RT)-RPA solution, reverse primers and viral RNA samples into a microfluidic channel for direct amplification. ZIKV and MERS-CoV RNAs were prepared using a commercial kit at a concentration range of 1 to $10^9$ copies/reaction (Fig. 5C). A 60 μL reaction mixture including 20 μL of viral RNA was injected into the microfluidic channel at 43 °C on the disk resonator after which the ZIKV target RNA was clearly distinguishable from either MERS-CoV or distilled water non-targets within 30 min (Fig. 5a). The signal trend of $10^4$ copies/reaction in the first 10 min looked different from the signal trends of other concentrations of viral RNAs, which may be due to the stabilization problem of the sensor, or RNA on the sensor, in the first 5 min (Fig. 5a). RNA is less stable molecule than DNA and requires time to react with other molecules including polymerase and enzymes on the sensor. Nevertheless, we successful used the resonator

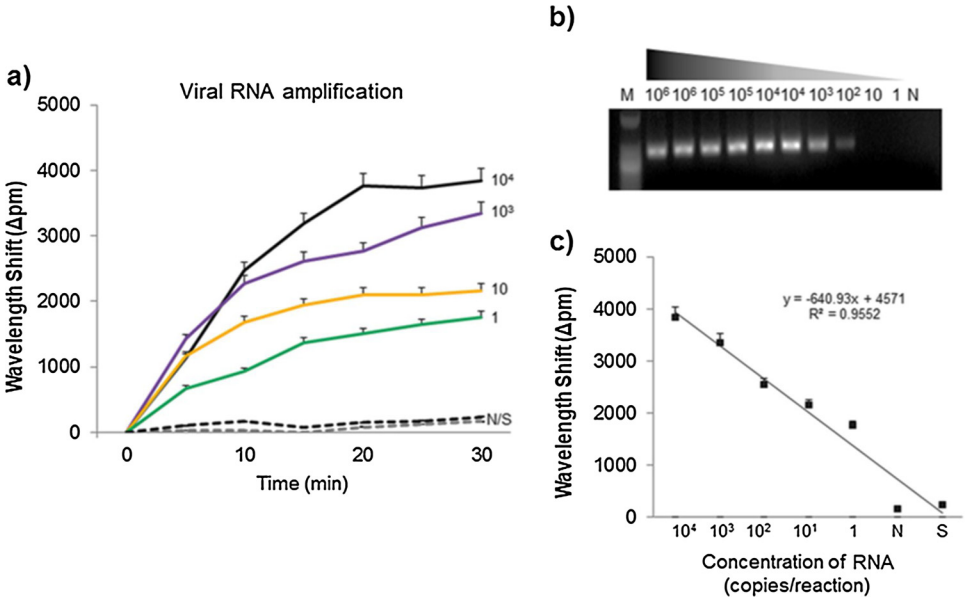


**Fig. 5.** Limit of detection of the nano-gap disk resonator for viral RNA amplification. a) A wavelength shift in the resonant mode is induced by serial dilutions of ZIKA virus RNA samples: black ($10^4$ copies/reaction), purple ($10^3$ copies/reaction), yellow (10copies/reaction), green (1 copy/reaction), black-dot (negative control containing no RNA), and gray-dot (negative control containing MERS-CoV RNA). b) Gel electrophoresis of 189 bp products generated by conventional quantitative reverse transcriptase (qRT)-PCR. M, 100bp marker; N, negative control with no RNA). c) Linear relationship between the wavelength shift in the resonant mode and the target RNA concentration within 30 min of the reaction commencement. Error bars indicate the standard error of the mean based on at least three independent experiments. (For interpretation of the references to colour in this figure legend, the reader is referred to the web version of this article).

to qualitatively distinguish between positive (ZIKV) and negative (MERS-CoV and water) samples within 10 min due to the non-background signal in the negative controls.

We again compared the limit of detection using the resonator and conventional PCR for serially diluted ZIKV viral RNA samples ranging from 1 to $10^4$ copies/reaction (Fig. 5). The resonance peak shifts increased proportionally from 1 (1763.33 pm, green) to $10^4$ (3836.00 pm, black) copies/reaction and were clearly distinguishable from the deionized water (no template control, black dot) and MERS-CoV RNA samples (non-target control, gray dot) (Fig. 5a). In the conventional RT-PCR assay, the amplicons (189 bp) were not visible below the $10^2$ copies/reaction threshold (Fig. 5b). The peak change results showed good linearity with the sample concentrations ($R^2 = 0.9810$) over 30 min (Fig. 5c). As found for bacterial DNA detection, the limit of detection of the SRSN disk resonator for viral RNA amplification was also 100-fold lower than that of the conventional method (Fig. 5).

## 4. Conclusions

We here describe a novel nucleic acid amplification system based on a nano-gap embedded active WGM resonator that has potential application as a molecular diagnostic tool due to its rapidity and high sensitivity. This photoluminescence sensor enables label-free and real-time amplification and direct detection of either bacterial DNA or viral RNA on the resonator surface. We successfully tested this system on several emerging infectious pathogens, such as the MERS-CoV, ZIKV viruses and the bacterial species *Brucella ovis*.

Compared to the iNAD system that uses SMRs, our new system has many advantages that overcome the limitations of other resonators (Table 1). First, the active resonator does not require any direct physical contacts for coupling of the waveguide and optical fiber. The embedded nano-gap structure enhances the detection sensitivity in biological applications. Second, very low to negative background signals are obtained from non-specific binding using our new photoluminescence resonator. A target at very low concentrations can thus be far more readily distinguished from non-targets at a high degree of sensitivity. Third, this photoluminescence sensor can rapidly detect a single copy target within 10 min. Total sensing can be achieved within 30 – 40 min when this sensor is combined with sample preparation using the SLIM (simple and label-free pathogen enrichment via homobifunctional imidoesters using a microfluidic) system [17]. Lastly, our novel resonator can be combined with visible LED source instead of tunable lasers, which will allow a reduction in size of the entire system and its use as a point-of-care testing device. Further larger scale and more in-depth studies will be needed to validate the clinical utility of our method. We envision however that this photoluminescence sensor will show utility in the future as a rapid molecular diagnostic tool and be used to identify molecular pathogens in a variety of clinical settings.

**Table 1**
Comparison of the nano-gap active resonator with other resonators.

| Types | Nano-gap active resonator[a] | Disk resonator[b] | Ring resonator[c] |
|---|---|---|---|
| | 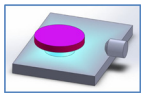 |  |  |
| Pump source | LED/CW laser | Tunable laser | Tunable laser |
| Coupling scheme | Light illumination in free-space | Tapered fiber | Bus waveguide |
| Primer state | Immobilized | Immobilized | Immobilized |
| Amplification condition | Isothermal (38 or 43 °C) | Not tested | Isothermal (38 or 43 °C) |
| Background signal | No | Yes | Yes |
| Target detection time | 10 min | 20 min | 20 min |
| Detection Limit (copies/reaction) | 10° | $10^1$ to $10^2$ | $10^1$ to $10^2$ |

[a] Optics Express 2019, 27(23), 34405; Current study.
[b] Sensors 2010, 10(10), 9317; IEEE Photonics Technology Letters 2013, 25(15), 1458; ACS Photonics 2017, 4, 2376.
[c] Laser Photonics Rev 2012, 6(1) 47; Lab Chip 2010, 10, 281; Sensors and Actuators B Chem 2013, 176, 552.

## Credit author statement

H. Lee and Y. Shin supervised the whole project and conceptualization. E.Y. Lee and Y. Kim conceived data curation and formal analysis. H. Lee and Y. Shin supported funding acquisition. E.Y. Lee, Y. Kim, B. Koo, and G.S. Noh supported investigation, methodology, resources, validation, and visualization of the data. E.Y. Lee, and Y. Kim wrote writing-original draft. H. Lee and Y. Shin wrote writing-review & editing. All authors read and approved the final manuscript.

## Declaration of Competing Interest

The authors declare that they have no known competing financial interests or personal relationships that could have appeared to influence the work reported in this paper.

## Acknowledgements

This study was supported by a grant from the Korea Health Technology R & D Project through the Korea Health Industry Development Institute (KHIDI), funded by the Ministry of Health & Welfare, Republic of Korea (HI16C-0272-010016), and also supported by a grant from the National Research Foundation of Korea funded by the Ministry of Science and ICT (2017R1C1B2011353, 2020R1A4A2002828 & 2020R1A2C2007148) Republic of Korea.

## Appendix A. Supplementary data

Supplementary material related to this article can be found, in the online version, at doi:https://doi.org/10.1016/j.snb.2020.128351.

## References

[1] V. Pinto, P. Sousa, S.O. Catarino, M. Correia-Neves, G. Minas, Microfluidic immunosensor for rapid and highly-sensitive salivery cortisol quantification, Biosens. Bioelectron. 90 (2017) 308–313.
[2] S.M. Yoo, S.Y. Lee, Optical biosensors for the detection of pathogenic micro- organisms, Trends Biotechnol. 34 (2016) 7–25.
[3] H. Šípová, S. Zhang, A.M. Dudley, D. Galas, K. Wang, J. Homola, Surface plasmon resonance biosensor for rapid label-free detection of microribonucleic acid at subfemtomole level, Anal. Chem. 82 (2010) 10110–10115.
[4] J.D. Driskell, A.G. Seto, L.P. Jones, S. Jokela, R.A. Dluhy, Y.P. Zhao, R.A. Tripp, Rapid microRNA (miRNA) detection and classification via surface-enhanced Raman spectroscopy (SERS), Biosens. Bioelectron. 24 (2008) 917–922.
[5] Y. Shin, A.P. Perera, K.W. Kim, M.K. Park, Real-time, label-free isothermal solid-phase amplification/detection (ISAD) device for rapid detection of genetic alteration in cancers, Lab Chip 13 (2013) 2106–2114.
[6] B. Koo, K.H. Hong, C.E. Jin, J.Y. Kim, S.H. Kim, Y. Shin, Arch-shaped multiple-target sensing for rapid diagnosis and identification of emerging infectious pathogens, Biosens. Bioelectron. 119 (2018) 79–85.
[7] G. Gaur, S. Hu, R.L. Mernaugh, I.I. Kravchenko, S.T. Retterer, S.M. Weiss, Label-free detection of Herceptin using suspended silicon microring resonaotors, Sens. Actuators B Chem. 275 (2018) 394–401.
[8] S. Hu, Y. Zhao, K. Q, S.T. Retterer, I.I. Kravchenko, S.M. Weiss, Enhancing the sensitivity of label-free silicon photonic biosensors through increased probe molecule density, ACS Photonics 1 (2014) 590–597.
[9] F. Vollmer, S. Arnold, Whispering-gallery-mode biosensing: label-free detection down to single molecules, Nat. Methods 5 (2008) 591.
[10] M.R. Foreman, J.D. Swaim, F. Vollmer, Whispering gallery mode sensors, Adv. Opt. Photonics 7 (2) (2015) 168–240.
[11] G.C. Righini, S. Soria, Biosensing by WGM microspherical resonators, Sensors (Basel) 16 (6) (2016).
[12] J.Y. Kim, B. Koo, C.E. Jin, M.C. Kim, Y.P. Chong, S.O. Lee, S.H. Choi, Y.S. Kim, J.H. Woo, Y. Shin, S.H. Kim, Rapid diagnosis of tick-borne illnesses by use of one-step isothermal nucleic acid amplification and bio-optical sensor detection, Clin. Chem. 64 (2018) 556–565.
[13] C.E. Jin, B. Koo, T.Y. Lee, K. Han, S.B. Lim, I.J. Park, Y. Shin, Simple and low-cost sampling of cell-free nucleic acids from blood plasma for rapid and sensitive detection of circulating tumor DNA, Adv. Sci. 5 (2018) 1800614.
[14] L. He, Y.F. Xiao, C. Dong, J. Zhu, V. Gaddam, L. Yang, Compensation of thermal refraction effect in high-Q toroidal microresonator by polydimethylsiloxane coating, Appl. Phys. Lett. 93 (2008) 201102.
[15] Y. Kim, H. Lee, On-chip label-free biosensing based on active whispering gallery mode resonators pumped by a light-emitting diode, Optic. Express 27 (2019) 34405–34415.
[16] H. Liu, F. Zhao, B. Koo, Y. Luan, L. Zhong, K. Yun, Y. Shin, 3 Dimethyl, 3′-dithiobispropionimidate (DTBP) as a cleavable disulfide- based polymer to encapsulate nucleic acids in biological sample preparation, Sens. Actuators B Chem. 288 (2019) 225–231.
[17] C.E. Jin, B. Koo, E.Y. Lee, J.Y. Kim, S.-H. Kim, Y. Shin, Simple and label-free pathogen enrichment via homobifunctional imidoesters using a microfluidic (SLIM) system for ultrasensitive pathogen detection in various clinical specimens, Biosens. Bioelectron. 111 (2018) 66–73.

**Eun Yeong Lee** received the M.S degree in University of Ulsan College of Medicine in 2019. His research is focused on development of molecular diagnostic platform based on optical biophotonics for detection of disease related biomarkers.

**Yeseul Kim** received her B.S. (2013) degree in Physics from Sogang University, Korea. Currently, she is pursuing a Ph.D. in Physics from Korea Advanced Institute of Science and Technology. Her interest is in design and fabrication of optical structure and its application in biological sensors.

**Bonhan Koo** received the M.S degree in University of Ulsan College of Medicine in 2018. He is a Ph.D student at University of Ulsan College of Medicine and Asan Medical Center, Seoul, Korea. His research is focused on development of molecular diagnostic platform based on optical biophotonics for detection of disease related biomarkers.

**Geun Su Noh** received the M.S degree in Sahm Yook University in 2017. He is M.S degree student at University of Ulsan College of Medicine and Asan Medical Center, Seoul, Korea. His research is focused on development of molecular diagnostic platform based on optical biophotonics for detection of disease related biomarkers.

**Hansuek Lee** is Assistant Professor in Graduate School of Nanoscience and Technology at KAIST and also Adjunct Professor in Department of Physics. He received his B.S., M.S., and Ph.D. degree in Electrical Engineering from Seoul National University in 2001, 2004, and 2008, respectively. From 2008 to 2015, he worked as a postdoctoral scholar, research staff, and visiting associate at California Institute of Technology (Caltech), Pasadena, CA. His research focuses on various nonlinear and quantum phenomena from visible to mid-IR wavelength range boosted by Ultra-High-Q resonators on a chip.

**Yong Shin** received the Ph.D. degree in Max Planck Institute of Experimental Medicine and Georg-August-University Goettingen, Germany in 2008. He is an Associate Professor at University of Ulsan College of Medicine and Asan Medical Center, Seoul, Korea. His research is now focused on development of molecular diagnostic platform based on optical biophotonics for detection of disease related biomarkers.